Numerical investigation on hydrodynamic performance of a novel shaftless rim-driven counter-rotating thruster considering gap fluid

Han Jiang[a], Wu Ouyang[a,b,c*], Chenxing Sheng[a,b,c], Jiafen Lan[a], Richard Bucknall[d]

[a] School of Transportation and Logistics Engineering, Wuhan University of Technology, Wuhan 430063, China
[b] Reliability Engineering Institute, National Engineering Research Center for Water Transport Safety, Wuhan 430063, China
[c] Key Laboratory of Marine Power Engineering and Technology, Ministry of Transport, Wuhan 430063, China
[d] Department of Mechanical Engineering, University College London, London WC1E 6BT, UK
*Corresponding author: ouyangw@whut.edu.cn

Abstract: Shaftless rim-driven thruster (RDT) has recently become the research focus for marine propulsion, primarily due to low vibration, low noise, and energy saving as its advantage. This study is based on CFD theory and used the Ansys-Fluent software to examine the hydrodynamic performance of a novel rim-driven counter-rotating thruster (RDCRT). It takes a No.19A+Ka4-70 duct propeller and a 20 kW RDT as examples, as it verifies the feasibility of the simulation method. It establishes three geometric models for RDCRT's hydrodynamic performance to determine whether it is necessary to consider the motor stator/rotor gap. It examines the flow distribution characteristics of the gap fluid friction force and flow channel and investigates the gap's influence on the hydrodynamic performance. Relevant case studies indicate that, when considering the gap, the calculation outcomes of the simulation model are between the stationary model and the rotational model of the rotor inner wall when ignoring the gap. In the Forward and Aft regions, the total frictional power of the gap channel correspondingly accounts for 1.7 % and 1.35 % of the rated power. Additionally, compared to situations with a gap, the pressure coefficient of the inner surface of the Forward and Aft rim without a gap is more significant. Thus, the hydrodynamic simulation model should not ignore the gap. For the RDCRT, the thrust coefficient, the torque coefficient, and the maximum efficiency value are more significant than those of the single-propeller RDT, hence validating its advantages.
Keywords: shaftless rim-driven thruster; counter-rotating propeller; hydrodynamic performance; gap fluid; friction torque

1 Introduction

The "Prime mover – Transmission system – Propeller" is the most prominent propulsion mode globally. Although this mode has excellent power, a mature design method, and manufacturing technology as its advantages, it likewise exposes various disadvantages alongside marine development. For example, the shafting penetrates through the submarines' pressure hull, enabling a high manufacturing cost and taking up much cabin space. Indeed, shafting vibration and noise are two of the stubborn diseases that restrict submarine stealth [1]. In this context, manufacturers devise the motor direct drive propulsion as a more advanced propulsion mode.

As a developing electric propulsion device, shaftless rim-driven thrusters (RDTs) incorporate rim-driving technology, depicted by the embed motor and propeller in a radial direction, thus eradicating the transmission shaft system. With the rapid progress of permanent magnet motor technology [2], hydrodynamic technology [3], and bearing technology, RDT realization is possible. Compared to a traditional propeller, an RDT saves around 15–25% cabin space [4] and exhibits low noise [5], flexible control (360° swiveling), and energy conservation [6]. Moreover, it applies to torpedoes, submarines, other applications that feature limited cabin capacity and high concealment requirement, yachts, civil vessels, underwater vehicles, and other related aspects. Consequently, several prominent international companies develop RDT products of different powers, including Rolls-Royce from the UK, Brunvoll from Norway, Schilling Robotics from the US, and Schottel and Voith from Germany.

Various scholars and relevant staff have expressed concern with propellers' high efficiency and energy conservation. Dollman and Perkins proposed a counter-rotating propeller (CRP) [7], which involves two propellers working opposite rotation directions on the same axis. Compared to an ordinary single propeller, CRP has several

advantages. Its rear propeller reuses the waste energy delivered by its front propeller's wake flow. When absorbing the same power, CRP's load is smaller than that of an ordinary single propeller, which is beneficial to avoid cavitation.

Meanwhile, a study proposed a novel design of a shaftless rim-driven counter-rotating thruster (RDCRT) to take advantage of the hydrodynamic performance of RDTs and CRP [8], as illustrated in Figure 1. The proposed model, which is highly compact, integrates two motors, the CRP's rim, and bearings into the duct. The two motors can undergo independent or uniform control and interact with each other. When one of these motors fails, the other can still stabilize the ship and push it toward a safe place at a low speed, thus enhancing the propeller's robustness.

Compared to a traditional propeller, the RDCRT has a significant difference in geometric structure. It is a combined hydraulic component, including a rim on the blade tip and a hollow in the blade root, leading to an apparent difference in flow field distribution between its two propellers. Relative to this, computational fluid dynamics (CFD) simulation analysis is more convenient and available than a direct experiment. Furthermore, it significantly saves costs. In this case, various research institutions welcome it. Based on CFD, various studies investigate CRP's hydrodynamic performance. Huang et al. [9] simulated the hydrodynamic performance of the CRPs in the effective wake using an in-house vortex-lattice code. The accuracy of the simulation method is verified by comparing with Reynolds-averaged Navier-Stokes (RANs) method. Wang et al. [10] found that the vessel with the hybrid CRP popped pulse showed a 17.59% large effective wave fraction, a 40.2% small thrust division fraction, and a 4.12% high overall productive efficiency compared with the single screen vessel through RANs method.

There is a connection in the gaps between the RDT motor and the bearing. As it works, the motor requires gap water to dissipate heat, while the bearing needs it for lubrication. Moreover, compared to the large-scale fluid around the propeller, the gap fluid's size is relatively small, bringing much difficulty to the fluid simulation. A closed natural water circulation channel will be formed by slotting the rim's front and rear ends and connecting with the gap between the motor rotor and stator. The gap has a positive effect on the motor's heat dissipation. Likewise, some problems exist, which are caused by the flow vortex when the fluid passes through a narrow flow channel. The rim surface can be divided into three parts - an outer surface, an inner surface, and an end surface - and applied various empirical formulae to predict the three friction moments. Based on RANs theory, Cao et al. [11] calculated and determined that the torque value of the inner surface was the largest and that the end surface was the most minor when using the CFD method. Then, Liu et al. [12] applied the same method to obtain the simulation results of the friction torque of the RDT gap channel and compared them with the analytical solutions. Applying numerical calculations, You et al. [13] calculated the gap flow of the ducted propeller and described in further detail the rule of the gap flow's influence on the mainstream field. Batten et al. [14] believed that, with a small radial gap, the Reynolds number was relatively small, and it was necessary to study the turbulent Taylor vortex with the Wilcox k-ω model having a low Reynolds number. Ke et al. [15] examined the gap flow rate, gap pressure difference, and the law of gap pressure difference when the rotating speed changed, and concluded that changing the fluid's shape in the gap could be an essential means to improve gap flow rate. Generally, the gap has a significant influence on the propeller's performance. Indeed, it is necessary to study the hydrodynamic model of the RDCRT considering such gaps, particularly to understand the interaction of the gap fluid between the front and rear blades of the RDCRT.

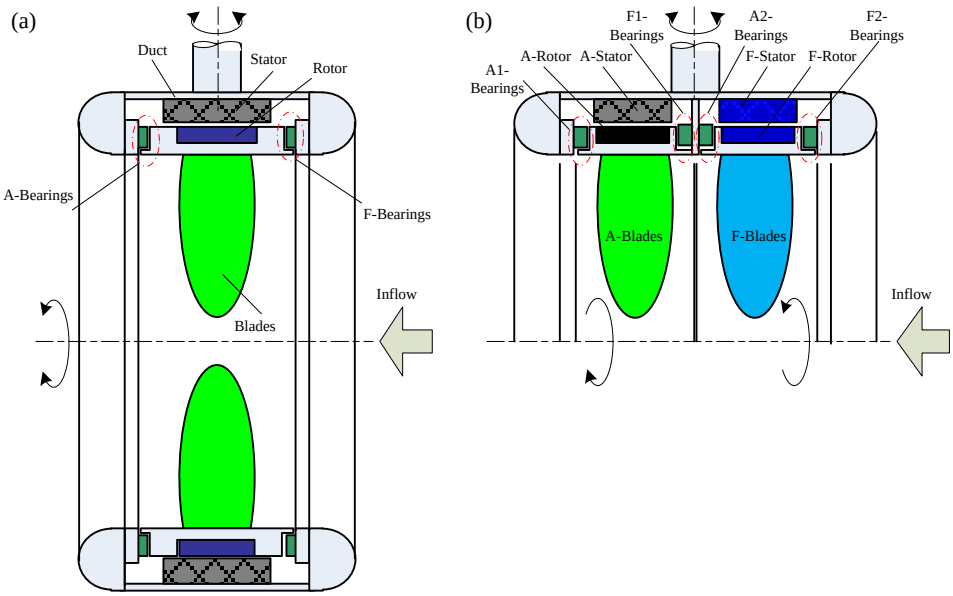

Fig. 1 Structure of the RDT: (a) single-propeller RDT; (b) RDCRT

For novel RDCRT, this study proposes and verifies a CFD-based hydrodynamic performance simulation method based on the Ansys-Fluent software. Employing a 20-kW CRT-RDT with two four-blade propellers and a diameter of 260 mm as the research object, it establishes three types of hydrodynamic simulation models of the CRT-RDT. It simulates gap fluid friction power consumption and the flow characteristics of the gap channel, and analyzes the gap's influence on the thruster's hydrodynamic performance.

2 Propeller performance simulation method

2.1 Basic equation

2.1.1 Governing equations

In this study, CFD solution is based on the basic governing equations of hydrodynamics which are composed of continuity equations and momentum conservation equations, and the Ansys-Fluent software was used as the solver to solve the equations, as shown below:

$$\begin{cases} \dfrac{\partial u_i}{\partial x_i} = 0 \\ \rho \dfrac{\partial u_i}{\partial t} + \rho \dfrac{\partial u_i u_j}{\partial x_j} = -\dfrac{\partial p}{\partial x_j} + \nu \dfrac{\partial}{\partial x_j}\left(\dfrac{\partial u_i}{\partial x_j} + \dfrac{\partial u_j}{\partial x_i} \right) + \dfrac{\partial}{\partial x_j}\left(-\rho \overline{u_i' u_j'} \right) \end{cases} \tag{1}$$

Where, t is the flow time. u_i, u_j (i,j=1,2,3) is the average velocity component. ρ is the density of water. p is the pressure. ν is the dynamic viscosity of water. $-\rho\overline{u_i' u_j'}$ represents the Reynolds stress.

2.1.2 The friction torque calculation model of the gap channel

The gap channel of the RDT is a small channel formed by motor stator, rotor (or rim) and bearing. It forms a closed channel with the large-scale channel of the duct, as shown in Figure 2. When the RDT rotor rotates, the radial gap fluid in the gap channel initiates a shearing effect, and the axial gap flow driven by the pressure difference between inlet and outlet will also initiate friction power consumption. So far, the most typical method is to divide the gap flow channel into two regional models respectively, namely the axial gap flow channel model and the radial gap flow channel model.

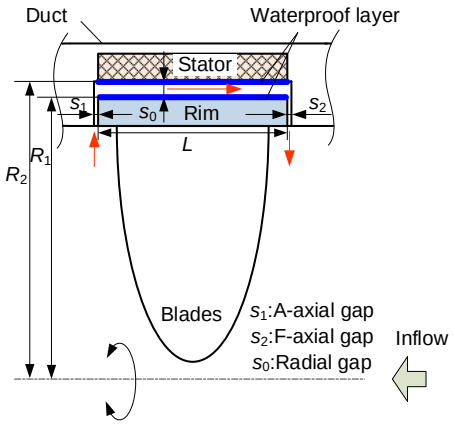

Fig. 2 Structure diagram of the RDT gap flow channel

(1) Analytical model of radial gap

The model proposed by Bilgen and Boulos [16] is used for the fluid friction moment of the radial gap, which combines their own experimental data and other scholars' research [17]. The model is divided into four states based on the size of the radial gap Reynolds number, and the calculation formula of radial gap torque is proposed as follow:

$$\begin{cases} M_r = 0.5\rho\pi\omega^2 R_1^4 L C_{Mr} \\ C_{Mr} = 10(H/R_1)^{0.3}\,\mathrm{Re}_r^{-1.0}\left(\mathrm{Re}_r \le 64\right) \\ C_{Mr} = 2(H/R_1)^{0.3}\,\mathrm{Re}_r^{-0.6}\left(64 < \mathrm{Re}_r \le 500\right) \\ C_{Mr} = 1.03(H/R_1)^{0.3}\,\mathrm{Re}_r^{-0.5}(500 < \mathrm{Re}_r < 10^4) \\ C_{Mr} = 0.065(H/R_1)^{0.3}\,\mathrm{Re}_r^{-0.2}(\mathrm{Re}_r > 10^4) \end{cases} \tag{2}$$

Where, M_r is the radial gap torque value. $Re_r=\rho\omega R_1 H/\mu$. μ is the dynamic viscosity of water. H is the radial gap height. ω is the angular velocity. R_1 is the radius of the outer wall of the rotor. L is the rim length. C_{Mr} is the radial gap moment coefficient. R_2 is the inner diameter of the stator.

(2) Analytical model of axial gap

The analytical model proposed by Daily et al. is used to solve the problem of friction torque for axial gap fluid [18]. The friction torque of a closed disc was measured with different Reynolds numbers at different axial gap ratios which were divided into four flow domains according to the range of the axial gap ratio and the axial gap Reynolds number [19]. The value of the RDCRT studied is within the range of 0.01-0.05, and the axial gap torque value M_a is calculated with following equations:

$$\begin{cases} M_a = M_{a1} + M_{a2} = 0.5\rho\pi\omega^2 R^4 h\left(C_{Ma1} + C_{Ma2}\right) \\ C_{Ma1} = \dfrac{0.16}{\left(\frac{a_1}{R}\right)^{0.167}\mathrm{Re}_a^{\,0.25}};\; C_{Ma2} = \dfrac{0.16}{\left(\frac{a_2}{R}\right)^{0.167}\mathrm{Re}_a^{\,0.25}} \\ a_{r1} = a_1/R_1;\; a_{r2} = a_2/R_1 \\ \mathrm{Re}_a = \rho\omega R_1^{\,2}/\mu \end{cases} \tag{3}$$

Where, a is the width of the axial gap. h is the height of the rim. Re_a is the Reynolds number of the axial gap. C_{Ma} is the axial gap moment coefficient, and subscripts 1 and 2 indicate the forward and rear faces of rim respectively.

2.1.3 Hydrodynamic performance equation

The advance coefficient, forward propeller thrust coefficient and moment coefficient, aft propeller thrust coefficient

and moment coefficient, total thrust coefficient, total moment coefficient and efficiency are defined as follows:

$$\text{Advance coefficient:}\quad J=\frac{V_a}{nD} \tag{4}$$

$$\text{Forward propeller:}\quad K_{T1}=\frac{T_1}{\rho n^2 D^4},\quad K_{Q1}=\frac{Q_1}{\rho n^2 D^5} \tag{5}$$

$$\text{Aft propeller:}\quad K_{T2}=\frac{T_2}{\rho n^2 D^4},\quad K_{Q2}=\frac{Q_2}{\rho n^2 D^5} \tag{6}$$

$$\text{RDCRT:}\quad \begin{cases} T=|T_1|+|T_2|, Q=|Q_1|+|Q_2| \\ \eta=\dfrac{K_T}{K_Q}\cdot\dfrac{J}{2\pi} \\ K_T=K_{T1}+K_{T2}, K_Q=K_{Q1}+K_{Q2} \end{cases} \tag{7}$$

Where, V_a is the inlet velocity (m/s). n is the rotation speed (r/min). T and Q are thrust (N) and moment (N·m) respectively. K_T is the thrust coefficient. K_Q is the torque coefficient. η is the efficiency. Subscripts 1 and 2 represent the forward and aft propeller respectively.

3 Verification of simulation methods

3.1 Duct propeller test verification

Considering the structural similarities between a ducted propeller and an RDT, the existing experimental data of a No.19A+Ka4-70 ducted propeller [20] was employed to verify the simulation method in this study. Table 1 presents the fundamental geometric parameters of the Ka4-70 propeller. The model applies a geometric projection method. Meanwhile, Table 2 provides the experimental data of the No.19A+Ka4-70 ducted propeller at J=0.2.

Table 1 Main parameters of Ka4-70 propeller

Number of blades	D/mm	Hub diameter ratio	Disk ratio	P/D	N/r/min
4	250	0.167	0.7	1.2	600

Table 2 Experimental values of No.19A+Ka4-70 duct propeller

J=0.2	Total thrust coefficient K_T	Duct thrust coefficient K_{Td}	Total torque coefficient $10K_Q$
Experimental value	0.5632	0.2385	0.6531

Firstly, it is necessary to establish and mesh a calculation domain. A No.19A+Ka4-70 ducted propeller adopts a cylindrical calculation domain. Figure 3(a) illustrates its size, where D is the propeller's diameter. The computational domain has two parts - the outermost static domain, and the inner rotating domain. The rotating domain adopts a finer unstructured grid to adapt to more drastic changes in the flow field, refines the propeller's leading and trailing edges, and utilizes a smoothing function to improve the grid. Figure 3(b) presents the grid of the ducted propeller. Finally, the fluent adaptive grid function adjusts the grid so that the grid's first internal node falls into the turbulent area. The fluent adaptive grid function is a program that automatically estimates the meshing error and refines the mesh that comes with Fluent software. The approximate techniques are used to automatically estimate the errors caused by

meshing in a specific analysis type. Through this error estimation, the software can determine whether the mesh is sufficiently fine. If the result error exceeds expectations, the program will automatically refine the mesh to reduce the error. Y-plus must be between 11.5 and 400, and the number of grids must be around four million.

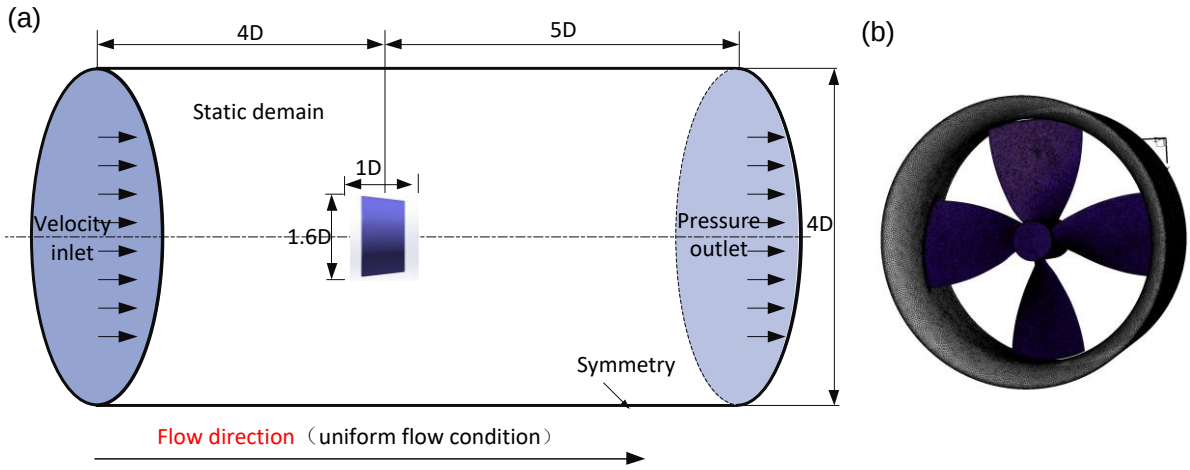

Fig. 3 Computational domain and grid

Boundary conditions setting is the second work of calculation. The inlet and outlet are set as velocity boundary and pressure boundary respectively. The contact surface between the static domain and the rotating domain selects the interface. The solution model can be divided into three parts: setting the algorithm, setting the discrete format and selecting the turbulence model. The SIMPLEC algorithm is used. The unstructured grid and Second order upwind method are applied to solve the fluid model.

According to the characteristics of RDT's hydrodynamic performance, four kinds of turbulence models - Standard *k-ε*, RNG *k-ε*, Realizable *k-ε*, and SST *k-ω* - are compared. Figure 4 presents the comparison between the simulation values and the experimental data of the total thrust coefficient, duct thrust coefficient (K_{Td}) and total moment coefficient when J=0.2. ΔK_{Td} is the error percentage of the duct thrust coefficient, ΔK_T is the error percentage of the total thrust coefficient, ΔK_Q is the error percentage of the total torque coefficient.

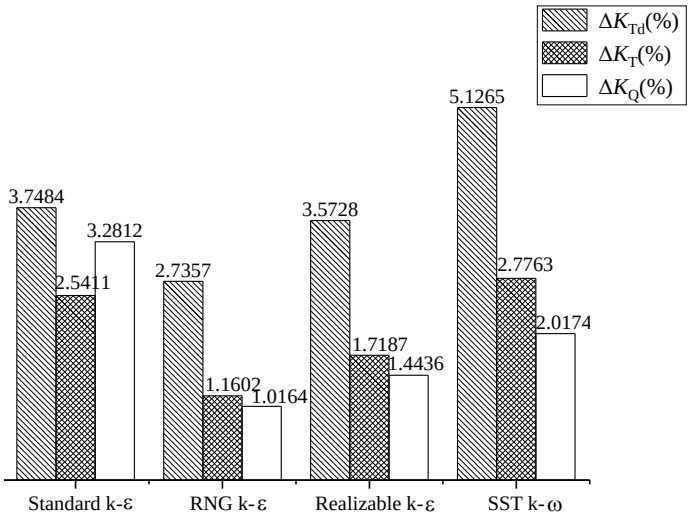

Fig. 4 Thrust and torque coefficient error diagrams of four turbulence models

From Figure 4, the simulated values of the ducted propeller are slightly larger than the experimental values. The total thrust coefficient error is less than 2.78%, while the total torque coefficient error is less than 3.3%. It manifests that the four turbulence models have reliable predictions for the ducted propeller's hydrodynamic performance.

However, the error is the smallest when using the RNG *k-ε* turbulence model, which is closer to the experimental values. Therefore, this study applies the RNG *k-e* turbulence model.

3.2 Test verification of RDT

This study selects 20-kW RDT for experimental verification to verify RDT's simulation method further. Figure 5 illustrates the circulating water tank used in the test. It is a horizontal water tank with a steel base and a glass wall, which can simulate the experimental environment of both ship engineering and ocean engineering. A double-sided laminated glass is applied in the test sections to observe flow field phenomena. The water depth of each test section is 1.2 meters. The maximum inflow velocity is 1.5 m/s. The maximum wave height is 0.3 meters. The regular wave period is 0.5-4 s. It includes a flow generation test section and a wave generation test section. The RDT test conducts in the flow section.

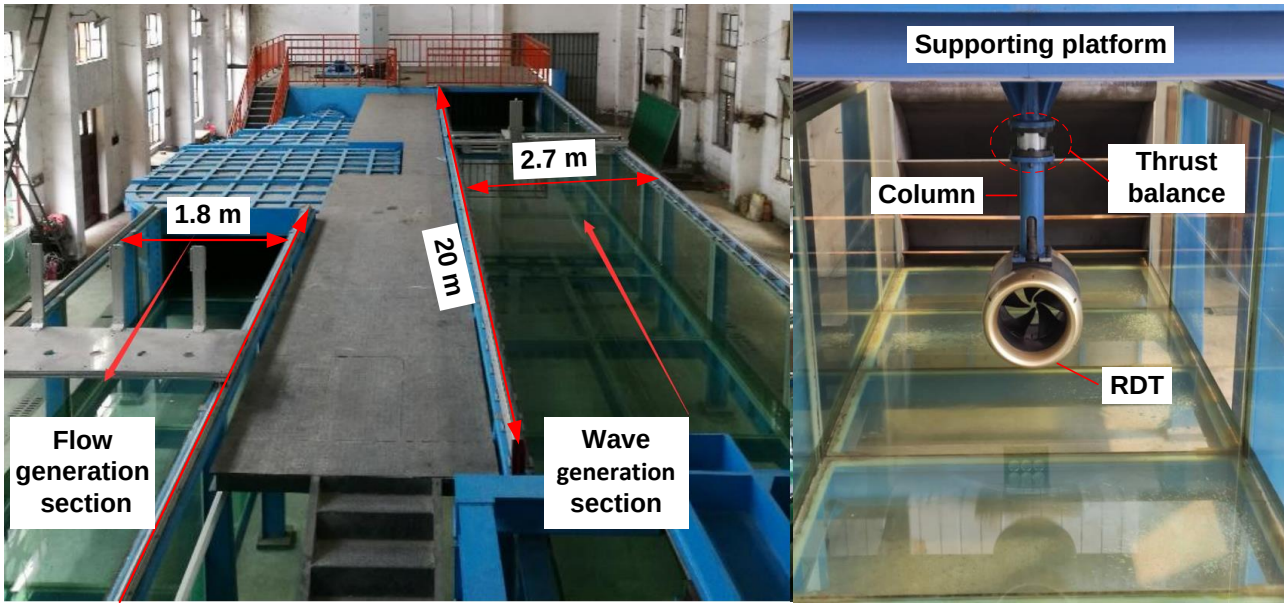

Fig. 5 The circulating water tank and test RDT

The propeller's diameter in an RDT test is 260 mm, and the rated rotational speed is 1680 r/min. Table 3 presents the RDT's detailed parameters, while Figure 5 illustrates the physical model. The blade tip of the RDT mounts on the inner wall of the rim, and no hub is present. Therefore, measuring thrust and torque using a traditional dynamometer is not suitable for the RDT. This test adopts the thrust balance based on the lever principle. It can output two-component forces, including axial force and torque. A column connects the RDT and the thrust balance. The thrust generated by the RDT acts on the thrust balance through the column, while the thrust balance converts the deformation into a voltage signal, eventually collected by a dynamic strain gauge (TST5811, Test Tlectronic Co., Ltd., China). Prior to the test, the thrust balance underwent calibration to obtain the relationship between voltage and thrust. After calibration, the thrust balance, column, and RDT are installed on the supporting platform such that the propeller's axis line is 640 mm away from the water surface, 560 mm away from the pool bottom, and the water depth is 1.2 m. At the beginning of the test, the initial signal is zero. Afterward, it is necessary to adjust the incoming flow speed. The RDT's rotational speed begins from 100 r/min, then increases 200 r/min every time. The thrust and torque require documentation at each speed.

Table 3 Parameters of blades and motor of 20kW RDT

Parameter	Value	Parameter	Value
Number of blades	5	Motor Power/(kW)	20
Blade diameter /(mm)	260	Rated voltage/(V)	288.5

Disk ratio	0.8	Rated current/(A)	43.8
Blade rake angle/(°)	40	Power factor	0.994
Hole-diameter ratio	0.1	Number of pole pairs	12
Rake angle of blade/(°)	0.11	Propeller material	NAB/Cu3

When inflow velocity is 0.21 m/s, the simulation value of the RDT's thrust coefficient is compared with the test value, as indicated in Figure 6. The simulation and experimental values of the thrust coefficient are consistent with the changing trend of rotational speed, increasing slowly alongside an increase in speed. However, there are a few differences between them. On the one hand, due to the structural strength of the connecting column, a higher rotational speed denotes an easier propeller and the vibration of the column, resulting in fluctuations of the thrust measurement value. On the other hand, the RDT simulation model does not consider the effect of the motor gap and water-lubricated bearing gap's friction power consumption, resulting in the simulation results being slightly larger than the experimental results. However, overall, the simulation results are still close to the experimental results, implying that the RDT simulation method used in this paper has good accuracy. This method can explore the hydrodynamic characteristics of the RDCRT.

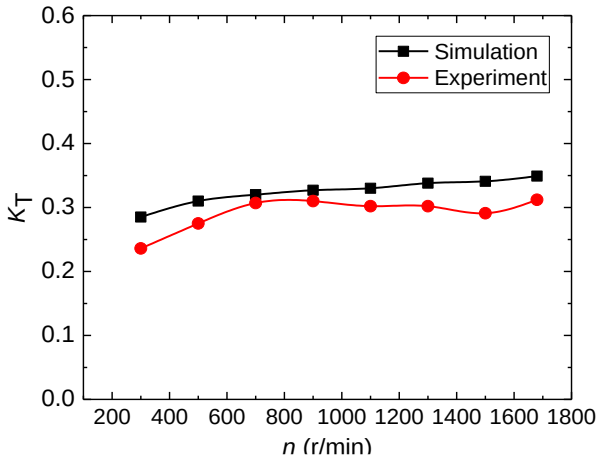

Fig. 6 Comparison of simulation and experimental results of RDT hydrodynamic performance

4 Simulation analysis of RDCRT gap flow

4.1 Geometric model

There are three methods in RDT modeling. The first is to model the rim and the propeller as a whole without considering the duct [21]. However, the calculation results are highly in contrast with the experimental ones due to the lack of duct. Therefore, researchers generally abandon them. The second method considers the duct but ignores the gap, which integrates the duct and the blade as a whole [22]. The third method considers the existence of ducts and gaps to establish the blade and the rim models, respectively [23]. In this study, the 2×10kW RDCRT was taken as the research object to establish two models-the gap and gapless models. Table 4 provides the specific parameters.

Table 4 Parameters of blades and ducts of 2×10kW RDCRT

Parameter	Value	Parameter	Value
Number of blades	4	Outer diameter of rim/(mm)	275
Hole-diameter ratio	0.1	Duct inner diameter /(mm)	300
Blade diameter/(mm)	260	Duct outer diameter/(mm)	408
Disk ratio	0.35	Duct length/(mm)	286
Pitch ratio	1.3	Duct thickness/(mm)	54
Radial gap/(mm)	1	Axial gap/(mm)	2

Rotational speed/(r/min)	1450	Rim thickness/(mm)	21

The duct's shape considers the shape of a JD7704 duct. However, due to the counter-rotating propeller's size and the motor's thickness, the duct's dimensions are modified accordingly. Figure 7 presents this modification.

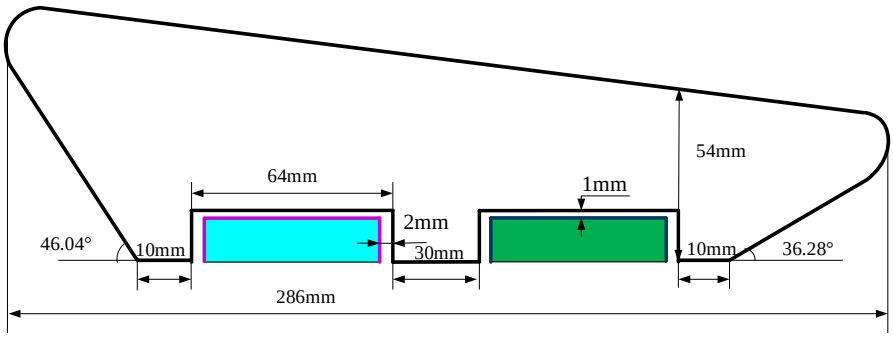

Fig. 7 Duct and gap size of the case

The radial and axial gaps of the RDT case are relatively small, mainly due to some reasons. The radial gap does not consider the size of the can of the motor stator and rotor, but only that of the interstitial fluid channel, which is relatively small. If the gap channel's size is too large, it can significantly impact the RDT's hydrodynamic performance. As size increases, the loss in the gap likewise increases, while the efficiency of the entire propeller decreases [19].

The comparison of a traditional RDT (single-propeller) and a RDCRT helps to explore the advantages of the latter. It is necessary to select a single propeller with the same effect as the CRP. In actual analysis, equivalent treatment is required. While keeping the blade form and pitch unchanged of two kinds of thruster, if the extension contour area of the CRP is equal to that of a single propeller, it can be considered that they are approximately equivalent. That is, A_E=A_{E1}+A_{E2}, where A_E, A_{E1} and A_{E2} are the extended contour areas of the single propeller, the forward and the aft propeller of CRP, respectively. The equivalent single propeller and the RDCRT have the same number of blades and diameters. The motor's rated power is proportional to the rotor's length when the stator's inner diameter, rated speed, and motor efficiency remain unchanged. The rated power of the RDCRT is 20 kW. Therefore, the rated power of the single-propeller RDT is 20 kW. Meanwhile, the radial gap, the axial gap, the duct length, and the maximum outer diameter are consistent with those of the RDCRT. Table 5 presents the final parameters of the equivalent single-propeller RDT, while Figure 8(c) illustrates the 3D model.

Table 5. Parameters of 20kW equivalent single propeller of RDT and duct

Parameter	Disk ratio	Pitch ratio	D/(mm)	Number of blades	Duct length/(mm)	Duct thickness/(mm)
Value	0.7	1.3	260	4	286	54

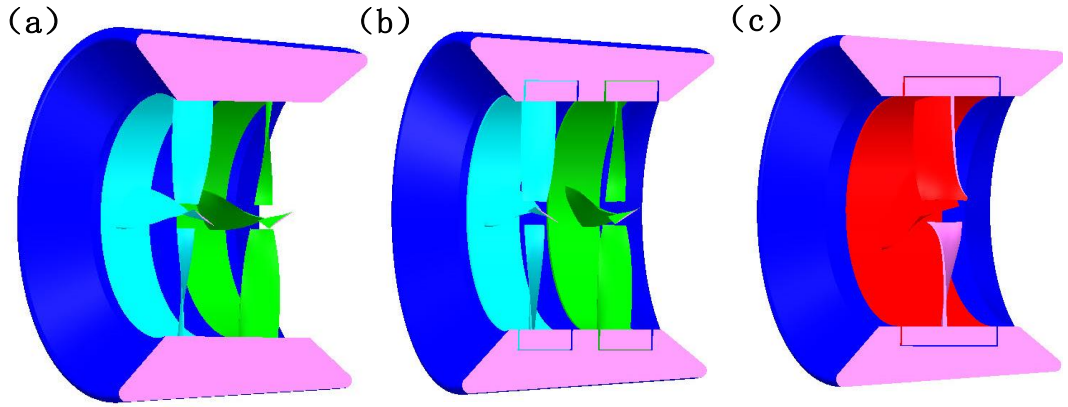

Fig. 8 3D models: (a) RDCRT without gaps; (b) RDCRT with gaps; (c) Traditional RDT with gaps

4.2 Discretization of the computational domain

The setting method of the calculation domain is the same as with Figure 3, where *D* refers to the maximum outer diameter of the RDT. The mesh module divides the mesh to refined it at the tip of the blade and the gap flow channel. Moreover, a boundary layer captures the characteristics of the flow field near the pipe. The grid is further adjusted through the fluent adaptive grid function such that the Wall Yplus of each part of the thruster meets 11.5<Y+<400. Figure 9 illustrates this grid. Based on the grid independence test, the grids of the front domain(the rotation domain where the Forward blade is located), the back domain(the rotation domain where the Aft blade is located), and the outer domain(static domain) are 2.88 million, 3.02 million, and 6.5 million, respectively.

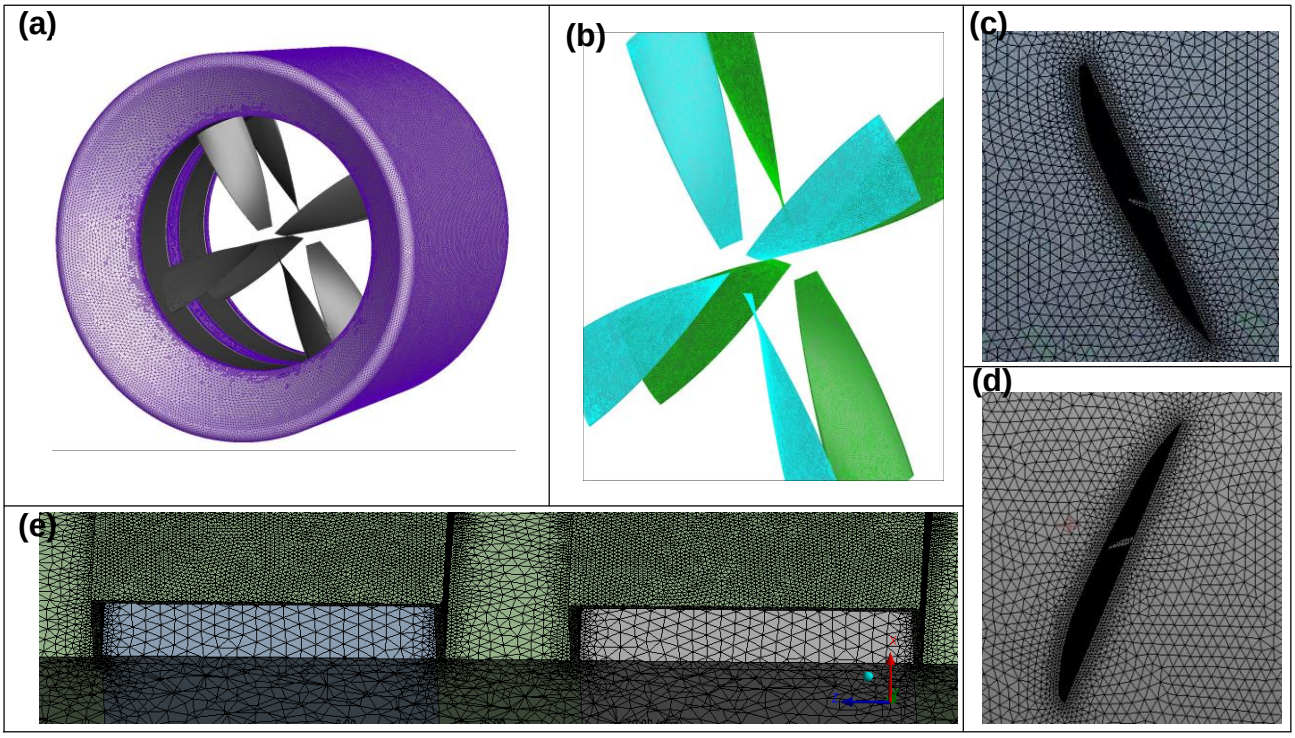

Fig. 9 Grid diagram of the RDCRT: (a) Thruster; (b) Blades; (c) Forward blade tip; (d) Aft blade tip; (e) Gaps

4.3 Friction torque and power consumption of gap flow

This study applies the RNG *k-e* turbulence model and the SIMPLEC separation solver to calculate the RDCRT's hydrodynamic force. At the same time, it applies the analytical model of the gap flow to calculate the friction torque on the outer surface and the front and rear ends of the forward and aft rims, from which it compares the experimental results with the numerical simulation values. As illustrated in Figure 10, In-duct, Ext-duct, and Out-duct represent the inlet axial gap wall, the radial gap wall, and the outlet axial gap wall of the duct. Meanwhile, In-rim, Ext-rim, and Out-rim represent those of the rim. Numbers 1 and 2 indicate the forward and aft gap flow, respectively.

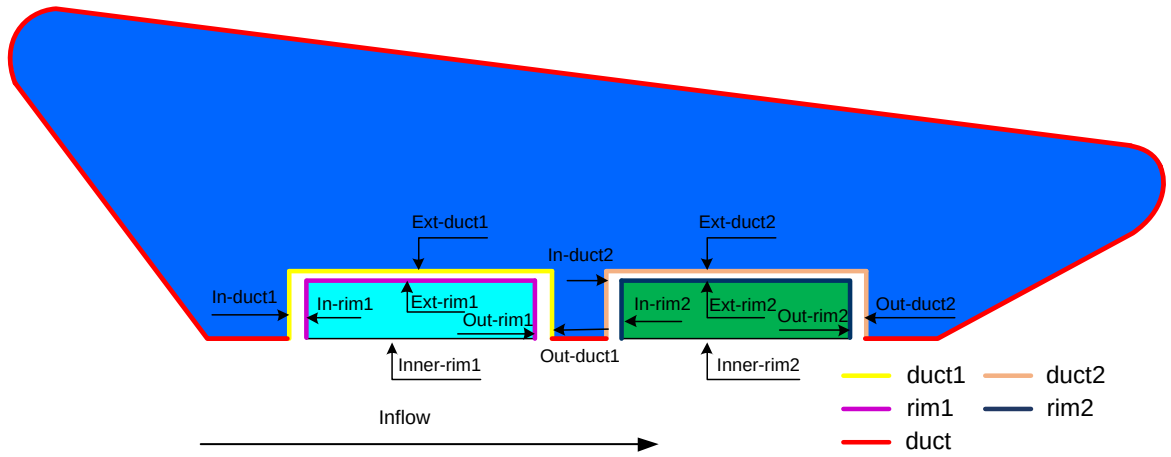

Fig. 10 The name of RDCRT gaps

At varying inlet velocities (0-7 m/s), the CFD simulation solution is solved to obtain the moment value of each gap surface, as shown in Tables 6 and 7. When the forward gap moment shares the same direction with the forward propeller moment, it is positive. Otherwise, it is negative. Meanwhile, when the aft gap moment shares the same direction with the aft propeller moment, it is positive. Otherwise, it is negative. In this sense, the friction moment's direction between the duct wall and the rim wall in the gap channel is opposite. The changing trend of the friction torque between the In-rim and the In-duct is opposite to the inlet velocity. Additionally, the friction torque of the Out-rim and Ext-rim decreases with an increase in velocity. Meanwhile, that of the Out-duct and Ext-duct increases alongside such an increase. In that case, the absolute value of the total torque slightly increases with an increase in velocity. This phenomenon is precisely the opposite of the change law of the torque at the rim, which is opposite to the variation of the rim's torque.

Table 6 Friction torque of rim wall in the gap channel (unit: N·m)

V_a(m/s)	In-rim1	Ext-rim1	Out-rim1	In-rim2	Ext-rim2	Out-rim2	Rim1	Rim2
0	0.4577	3.5202	1.1567	0.6693	2.7262	0.9914	5.1346	4.3868
1	0.4622	3.5164	1.1490	0.6745	2.7227	0.9800	5.1276	4.3771
2	0.4675	3.4781	1.1407	0.6813	2.7027	0.9711	5.0863	4.3551
3	0.4723	3.4400	1.1302	0.6842	2.6785	0.9529	5.0426	4.3156
4	0.4772	3.4029	1.1293	0.6892	2.6538	0.9344	5.0093	4.2773
5	0.4821	3.3576	1.1267	0.6900	2.6303	0.9036	4.9664	4.2239
6	0.4865	3.3003	1.1168	0.7004	2.6095	0.8672	4.9036	4.1770
7	0.4902	3.2370	1.1140	0.7167	2.5913	0.8188	4.8412	4.1268

Table 7 Friction torque of the duct wall in the gap channel (unit: N·m)

V_a(m/s)	In-duct1	Ext-duct1	Out-duct1	In-duct2	Ext-duct2	Out-duct2	Duct1	Duct2
0	-0.6362	-1.9805	-0.1951	-0.5425	-2.5687	-0.2657	-2.8118	-3.3769
1	-0.6317	-1.9861	-0.1981	-0.5413	-2.5868	-0.2712	-2.8159	-3.3993
2	-0.6265	-2.0081	-0.2012	-0.5409	-2.6099	-0.2772	-2.8357	-3.4280
3	-0.6221	-2.0300	-0.2053	-0.5370	-2.6349	-0.2882	-2.8574	-3.4600
4	-0.6179	-2.0523	-0.2055	-0.5347	-2.6590	-0.3011	-2.8756	-3.4948
5	-0.6137	-2.0803	-0.2080	-0.5232	-2.6669	-0.3209	-2.9020	-3.5109
6	-0.6099	-2.1172	-0.2113	-0.5148	-2.6817	-0.3451	-2.9384	-3.5415
7	-0.6071	-2.1992	-0.2115	-0.4948	-2.7021	-0.3783	-3.0178	-3.5752

Fig. 11 provides summing up the friction torques to obtain the total torque. Total1 refers to the sum of Rim1 and

Duct1, while Total2 refers to the sum of Rim2 and Duct2. Indicatively, the friction torque of Rim1 is greater than that of Rim2, while the torque of Duct1 is less than that of Duct2. Moreover, Total1 is slightly greater than Total2. Generally, the existence of the gap channel slightly increases the total torque loss of the propeller, and decreases with the increase in inlet velocity. That is, when V_a = 0 m/s (mooring state), the torque loss of the gap flow channel reaches its maximum value.

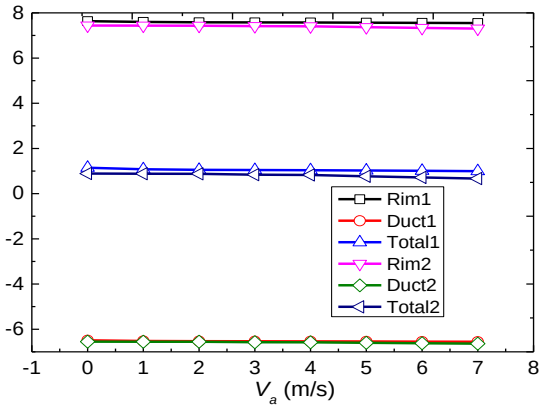

Fig. 11 Total friction torque of gap flow channel (unit: N·m)

From Table 8, when V_a = 0 m/s, the friction power consumption P_m of the rim and duct in the gap flow channel, and the rated power P_0 of a single motor is 10 kW. The rim's power losses in the forward and aft gap channels account for 11.59% and 11.29%, respectively. Since the duct's wall surface in the gap channel can generate a moment in the opposite direction to the rim, the rim's friction torque can ensure balance. Thereafter, the total friction power consumption of the forward and aft gap channels account for 1.7% and 1.35%, respectively, thus effectively reducing the propeller's power loss.

Table 8 Friction power consumption of gap flow channel

	M （N·m）	P_m（kW）	P_m/P_0
Rim1	7.63499	1.15932	0.11593
Duct1	-6.48972	0.98542	0.09854
Total1	1.14527	0.17390	0.01739
Rim2	7.43961	1.12966	0.11297
Duct2	-6.54976	0.99454	0.09945
Total2	0.88985	0.13512	0.01351

Fig.12 provides a comparison between the CFD simulation solution and the analytical solution of the gap flow's friction torque when V_a = 0 m/s. In this case, there are differences between the two solutions on each of the rim's surfaces. The relative differences were 3.88% and 11.8%, respectively. The total friction moments of the solutions are the same, except that the local gaps are different. For RDCRT, the flow generated by the forward and aft propellers influence each other. Consequently, the fluid boundary conditions in the forward and aft gap flow channels are different. The analytical solution cannot express the flow difference between the forward and aft gaps. Hence, the CFD method is relatively accurate.

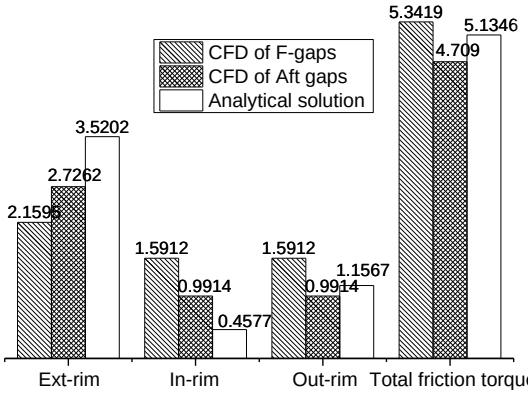

Fig. 12 Numerical and analytical solutions of rim friction torque (unit: N·m)

4.4 Flow characteristics of gap flow

The gap channel's flow characteristics are analyzed to determine further the difference in friction power consumption between the forward and aft gap flows. Figure 13 presents the gap's pressure distribution. It illustrates that the pressure difference between the front and rear blade surfaces results in a pressure difference between the inlet and outlet of the gap fluid when the propeller rotates. Since the pressure difference between the front and rear surface of aft blades is more significant than the forward blades, the pressure distribution in the aft gap channel is greater than that of the forward gap. The analytical model of the gap flow's friction torque considers only rotation, and excludes gap pressure difference. Thus, the prediction error of friction torque in the aft domain is more significant than that in the forward domain.

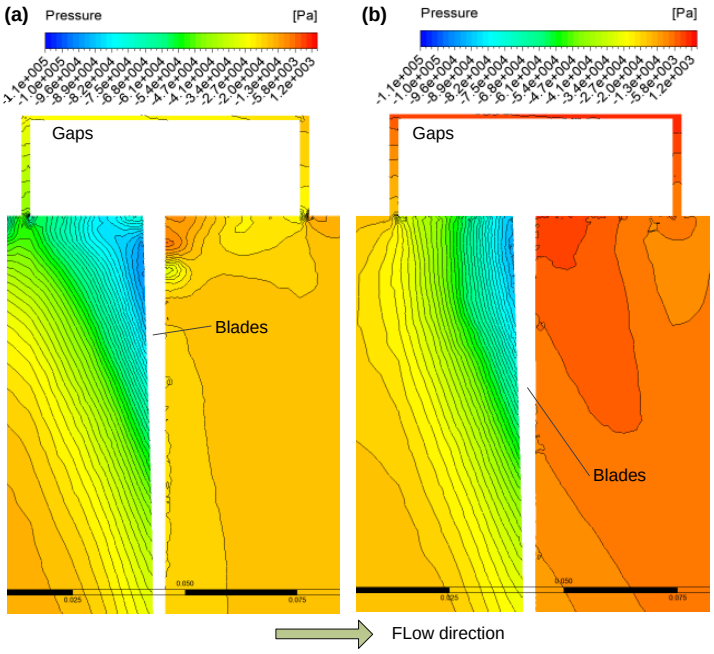

Fig. 13 Pressure distribution: (a) Froward domain; (b) Aft domain

Figure 14 presents the fluid velocity distribution in the gap channel, indicating that with the propeller's rotation, the closer to the rim wall, the greater the flow velocity. Considering that the aft propeller absorbs the wake energy of the forward propeller, low-speed vortices exist on the inner surface of the forward rim, and the velocity on the inner surface of the aft rim is larger and more uniform. Figure 15 depicts the axial velocity vector diagram of the fluid in the forward gap channel. Due to pressure difference, the flow in the gap is opposite to the propeller's flow direction.

The gap flow and the propeller flow form a closed loop, resulting in a local fluid “short circuit.” This phenomenon loses part of the blade backpressure, which is unfavorable for efficiency.

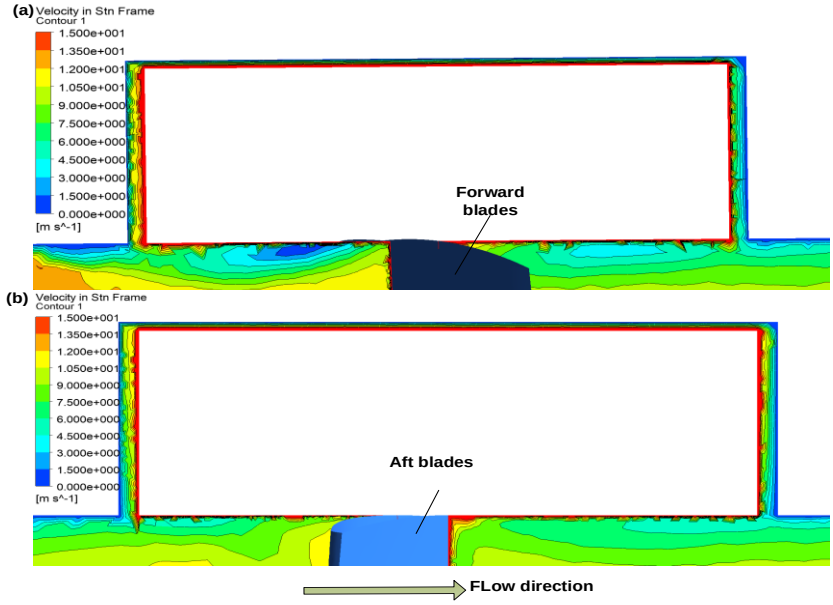

Fig. 14 Gap fluid velocity distribution: (a) Forward domain; (b) Aft domain

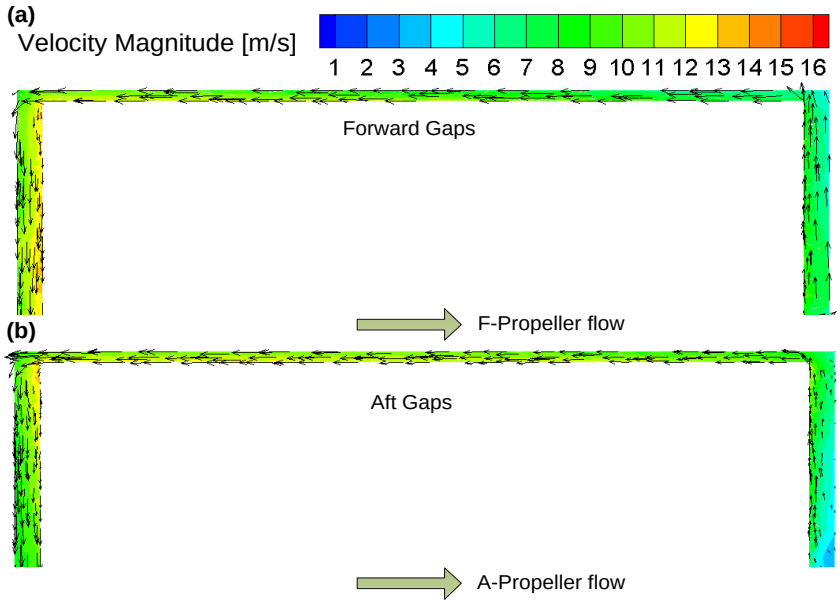

Fig. 15 Fluid velocity vector distribution of gap fluid

Figure 16(a) presents the axial pressure distribution on the rim’s outer surface, where the Z-coordinate represents the inlet-to-outlet distance with the pressure coefficient as the ordinate: $C_p=(p-p_0)/(0.5\rho v^2)$. p_0 represents the reference pressure, while v represents the free flow velocity. The corresponding positions of the forward propeller and the aft propeller in the Z-coordinate are -51.3~-47 mm and 42.7 mm~47 mm. Although there is no pressure value in this position, Figure 16(a) connects this position to analyze the pressure difference of the blade tip section. The forward blade’s pressure coefficient at the blade tip section is smaller than that of the aft blade, proving that the aft blade absorbs the wake energy of the forward blade and increases the thrust. Moreover, regarding the pressure coefficient at the front and rear ends of the rim, the forward blade is smaller than the aft propeller. The pressure coefficient of the rim’s outer surface changes very little, signifying that the pressure distribution on the rim’s outer surface is

uniform and that the flow state is stable.

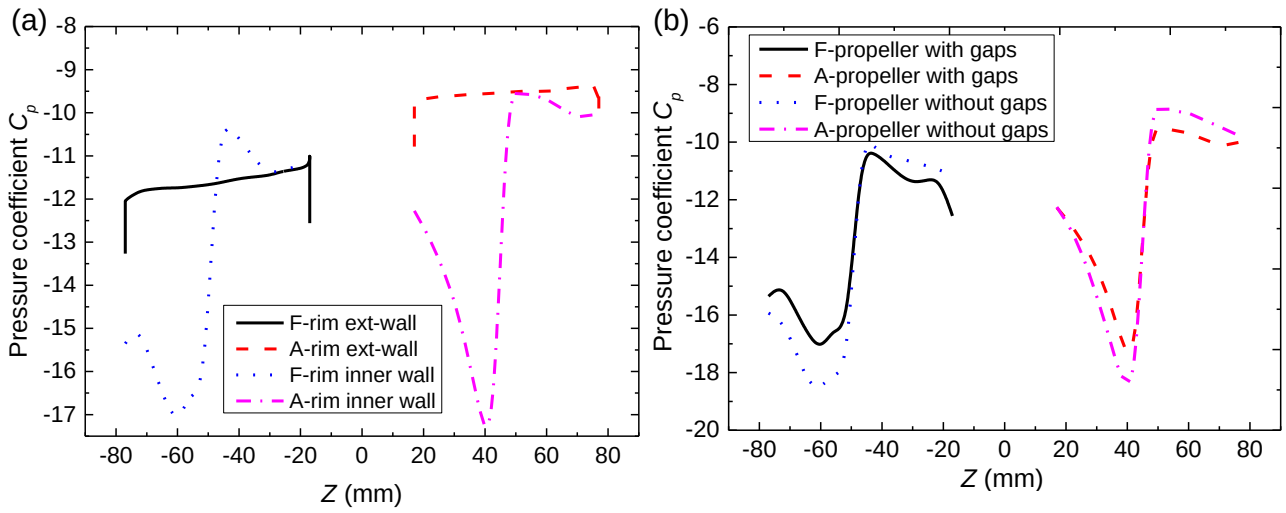

Fig. 16 Propeller local axial pressure distribution: (a) Outer surface of rim; (b) Inner surface of rim

Considering the gap or otherwise, the pressure distribution on the rim's inner surface further affects the parameters. As shown in Figure 16(b), the pressure coefficients of the inner rim surface from the models with and without gap are extracted. It signifies that, regardless of the gap, the pressure coefficient of the aft rim's inner surface is greater than that of the forward rim, proving that the aft propeller can absorb the forward propeller's tail flow energy. Meanwhile, when not considering the gap, the rim inner surfaces' pressure coefficients are more significant than those when considering the gap, indicating that ignoring the gap can result in a more considerable thrust prediction value. Thus, on the one hand, the gap channel causes power loss, and the friction power consumption of the gap fluid is essential. On the other hand, there are differences between the forward gap flow and the aft gap flow of RDCRT. However, the analytical solution of gap friction torque cannot transpire. Hence, the CFD numerical solution is relatively accurate.

5 Simulation analysis of RDCRT hydrodynamic performance

5.1 Effect of gap on hydrodynamic performance

There are two types of boundary conditions for the gapless model. That is, the inner surface of the rim is stationary in Model 1, while that of model 2 is rotatory. The model considering the gap is named Model 3. All three models are used to simulate the propeller's hydrodynamic performance. Figure 17 presents the comparison of the results.

In an extensive range of advance coefficients, the total thrust coefficient of Model 3 is the largest, followed by Model 1, while Model 2 is the smallest. The torque coefficients of the three models are significantly different. That is, Model 3 has the most considerable value, followed by Model 2, while Model 1 is the smallest. The efficiency of Model 1 is between that of Model 2 and Model 3. At a low advance coefficient, the efficiency of Model 1 is closer to that of Model 3. With an increase in advance coefficient, the efficiency difference obtained from the two models gradually increases. Thus, given the calculation accuracy of RDCRT hydrodynamic performance, the gap should not be ignored.

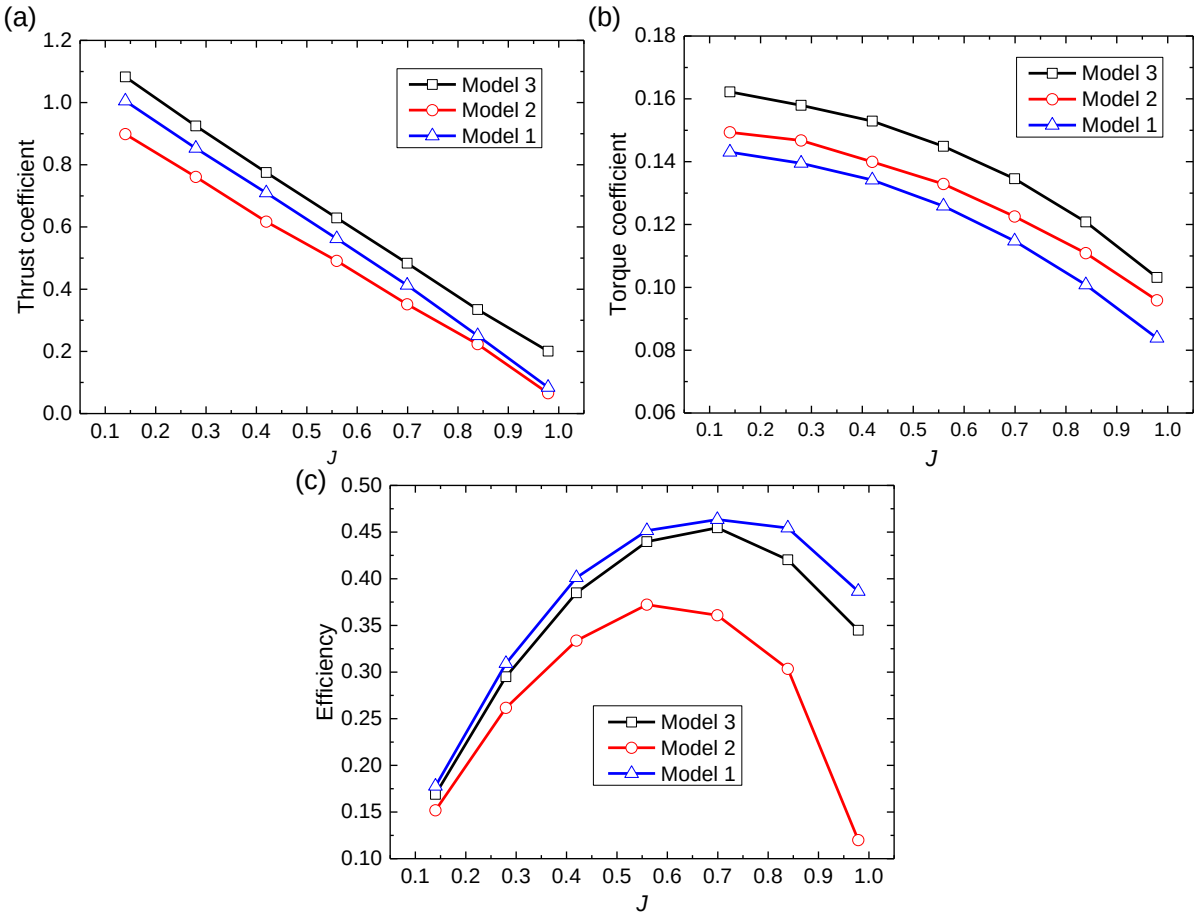

Fig. 17 Simulation results of three models: (a) Thrust coefficient; (b) Moment coefficient; (c) Efficiency

5.2 Numerical results by the gap model

Based on the CFD simulation solution with gaps, this study simulates the RDCRT and the single-propeller RDT. Table 9 and Table 10 present the thrust and torque of components of the RDCRT at varying inlet velocities. Blades1 refers to the forward propeller, Blades2 refers to the aft propeller, and Inner-rim1 and Inner-rim2 correspondingly refer to the inner surfaces of the forward and aft rims. T_1 and T_2 denote the total thrust values of the components in the forward and aft domains, respectively. Q_1 and Q_2 correspondingly signify the total torque value of the components in the forward and aft domains.

Table 9 Thrust of each component (unit: N)

V_a(m/s)	1	2	3	4	5	6	7
Duct	1167.7303	814.7827	508.8438	249.0052	21.8231	-178.1145	-387.7605
Inner-rim1	-1.0719	-1.3131	-1.6267	-1.9505	-2.2498	-2.5824	-2.9048
Baldes1	731.7420	702.4217	655.4316	596.7848	528.4626	447.0169	346.2755
Duct1	-451.0745	-443.6074	-426.3859	-407.9334	-391.1874	-368.7295	-347.4365
Rim1	447.9653	434.9012	418.1164	399.7803	383.2158	361.1263	340.1511
T_1	727.5609	692.4023	645.5353	586.6811	518.2412	436.8313	336.0853
Inner-rim2	-7.3914	-7.5049	-7.6706	-7.9006	-8.2367	-8.6068	-8.9562
Blades2	1003.6074	974.8394	927.4706	857.2568	763.5825	647.4033	601.6007
Duct2	-191.9479	-178.8659	-167.8233	-151.8314	-127.5166	-104.8497	-69.6698
Rim2	185.5888	172.9678	162.0580	146.2245	122.3029	99.6010	64.3563

T_2	989.8569	961.4364	914.0348	843.7493	750.1322	633.5478	587.3309

From Table 9, at varying inlet velocities, the thrust of Rim1 is always greater than that of Rim2. Moreover, the negative thrust generated by Inner-rim1 is always less than that by Inner-rim2. Meanwhile, the negative thrust generated by Duct1 is more significant than that by Duct2. As for the aft propeller, the generated thrust is always greater than that by the forward propeller. The total thrust of the aft domain is more significant than that of the forward domain. From Table 10, Duct1 and Duct2 generate a torque opposite to the blades in the same domain. All other components generate the torque in the same direction as the blades in the same domain. The torque of Rim1 is always greater than that of Rim2, while the torque of Inner-rim1 is always less than that of Inner-rim2. Meanwhile, the negative torque generated by Duct1 is always less than that by Duct2. Additionally, the torque generated by the aft propeller is always greater than that by the forward propeller. Hence, the total torque of the aft domain is more significant than that of the forward domain. Moreover, since the duct does not rotate, the proportion of its torque to the total torque is so insignificant that one can almost ignore it. It is why this study ignores duct torque in the conventional ducted propeller efficiency.

Table 10 Torque of each component (unit: N·m)

V_a(m/s)	1	2	3	4	5	6	7
Duct	-0.0636	-0.6096	-0.0578	-0.0519	-0.0506	-0.0420	-0.0361
Inner-rim1	2.1842	2.1909	2.1977	2.2554	2.3093	2.3900	2.4845
Baldes1	44.8099	43.5998	41.6029	39.0516	36.0088	32.1802	27.3481
Duct1	-2.8159	-2.8357	-2.8574	-2.8756	-2.9020	-2.9384	-3.0178
Rim1	5.1276	5.0863	5.0426	5.0093	5.1346	4.9036	4.8412
Q_1	49.3058	48.0413	45.9857	43.4407	40.5507	36.5354	31.6560
Inner-rim2	3.2965	3.3190	3.3482	3.3892	3.4410	3.5017	3.5468
Blades2	59.0538	57.9304	55.9808	52.9795	48.7436	43.2073	35.8740
Duct2	-3.3993	-3.4280	-3.4600	-3.4948	-3.5109	-3.5415	-3.5752
Rim2	4.3771	4.3551	4.3156	4.2773	4.2239	4.1770	4.1268
Q_2	63.3281	62.1765	60.1845	57.1512	52.8975	47.3444	39.9723

Figure 18 illustrates RDCRT's hydrodynamic performance. K_{T1} refers to the total thrust coefficient of the component in the forward domain, K_{Q1} denotes the total torque coefficient, K_{T2} entails the total thrust coefficient of the component in the aft domain, K_{Q2} refers to the total moment coefficient, and K_{T3} signifies the thrust coefficient of the duct. In comparison, K_T and K_Q, respectively denote the total thrust coefficient and total torque coefficient of the RDCRT. As the advance coefficient increases, K_{T1}, K_{T2}, K_{T3}, K_T, K_{Q2}, K_{Q1}, and K_{Q2} gradually decrease. K_{T3} decreases more drastically, making the total thrust coefficient K_T further decrease by a more considerable margin. With the increase of the advance coefficient, the duct's resistance gradually increases, and the duct attachment vortex caused by the propeller trailing vortex gradually decreases. In that case, the thrust generated by the duct decreases more sharply than that by the blades. The efficiency initially increases and then decreases with the increase of the advance coefficient. When J is 0.65, the efficiency reaches its maximum.

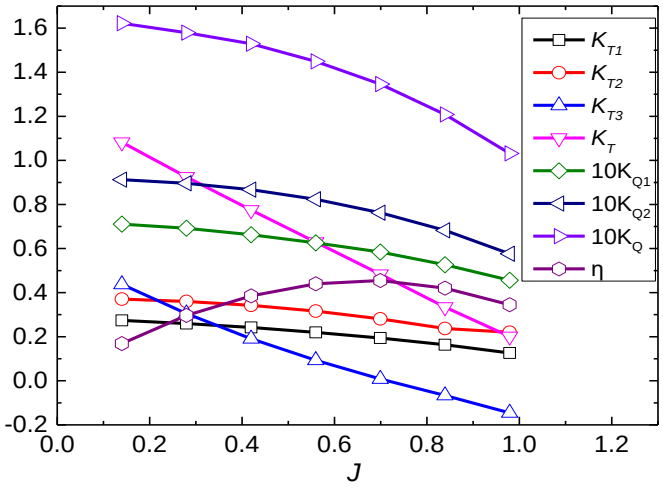

Fig. 18 Hydrodynamic performance of RDCRT

Figure 19 illustrates the hydrodynamic performances of the RDCRT and the single-propeller RDT. The thrust coefficient, torque coefficient, and efficiency of RDCRT are greater than those of the single-propeller RDT. Moreover, as the advance coefficient increases, the efficiency advantage of the RDCRT becomes more apparent. Since the rotation directions of the forward and aft propellers of RDCRT are different, the torque directions generated by them are also opposites, making the RDCRT balance the overturning torque and enhance its stability. However, due to the contra-rotation of the two propellers, the flow fields of the forward and aft propellers depict noticeable non-uniformity, resulting in periodic fluctuating pressure. In the follow-up studies, further noise research on RDCRT is necessary.

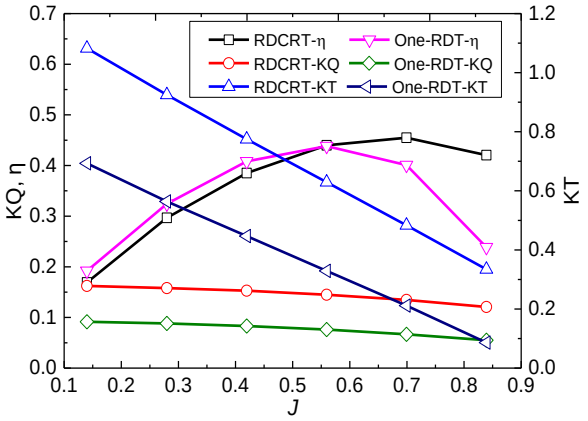

Fig. 19 Comparison of hydrodynamic performance of two RDT

6 Conclusions

This study conducts a simulation method considering gap fluid of RDT hydrodynamic performance. It implements a simulation of a 2×10kW RDCRT and analyzes the influence of gap flow on hydrodynamic performance. The following are the conclusions obtained:

(1) A CFD simulation model of the RDCRT is established. The numerical values of the friction torque of the forward and aft gaps differ from the analytical solutions by 3.88% and 11.8%, respectively. Influenced by the flow fields of two propellers, the flow characteristics of the forward and aft gap channels are also different. However, the analytical solutions cannot reflect this detail. In that case, the analytical method is not suitable for the RDCRT.

(2) The calculation results by the simulation model with a gap are between those by two gapless models with a stationary and rotatory rim inner surface. Neglecting such a gap can result in the thrust prediction value be more significant than considering the gap. Given the calculation accuracy of RDCRT hydrodynamic performance, the gap

is essential.

(3) The thrust and torque coefficients of the RDCRT are higher than those of the single-propeller RDT, as well as its maximum efficiency value.

Acknowledgment

This project was financially supported by National Key Research and Development Project of China (No. 2018YFE0197600) and the National Natural Science Foundation of China (No. 52071244).

References

[1] F. Chen, Y. Chen, H.X. Hua, Vibration analysis of a submarine elastic propeller-shaft-hull system using FRF-based substructuring method, J. Sound Vib. 443(2019) 460-482.

[2] S.M. Sharkh, S.H. Lai, Slotless PM brushless motor with helical edge-wound laminations, IEEE T. Energy Conver. 24(2009) 594-598.

[3] S. Gaggero, Numerical design of a RIM-driven thruster using a RANS-based optimization approach, Appl. Ocean Res. 94(2020) 101941.

[4] X.P. Yan, X.X. Liang, W. Ouyang, Z.Z. Liu, B. Liu, J.F. Lan, A review of progress and applications of ship shaft-less rim-driven thrusters, Ocean Eng. 144(2017) 142-156.

[5] S. Gaggero, G. Tani, M. Viviani, F. Conti., A study on the numerical prediction of propellers cavitating tip vortex, Ocean Eng. 92(2014) 137-161.

[6] M. Lea, D. Thompson, B.V. Blarcom, J Eaton, J Friesch, J Richards, Scale model testing of a commercial rim driven propulsor pod, J. Ship Production, 19(2003) 121-130.

[7] H. Ghassemi, M. Taherinasab, Numerical calculations of the hydrodynamic performance of the contra-rotating propeller (CRP) for high speed vehicle, Pol. Marit. Res. 20(2013) 13-20.

[8] X.P. Yan, W. Ouyang, Z.L. Liu, X.X. Liang, Counter-rotating shaftless rim drive thruster, China patent, 2015, CN 105109650 A. (in Chinese)

[9] Y.S. Huang, J. Yang, C.J. Yang. Numerical prediction of the effective wake profiles of a high-speed underwater vehicle with contra-rotating propellers, Appl. Ocean Res. 84(2019) 242-249.

[10] Z.Z. Wang, S.S. Min, F. Peng, X.R. Shen, Comparison of self-propulsion performance between vessels with single-screw propulsion and hybrid contra-rotating podded propulsion, Ocean Eng. 232(2021):109095

[11] Q.M. Cao, W.F. Zhao, D.H. Tang, F.W. Hong, Effect of gap flow on the torque for blades in a rim driven thruster without axial pressure gradient, Procedia Eng. 126(2015) 680-685.

[12] B. Liu, X.P. Yan, W. Ouyang, J.F. Lan, X.X. Liang. Research on regular pattern of gap flow in Shaftless Rim-driven thruster, Proceedings of the 4th International Conference on Transportation Information and Safety, ICTIS 2017, Banff, Alberta, Canada, 2017 134-138.

[13] D. You, M. Wang, P. Moin, R. Mittal, Large-eddy simulation analysis of mechanisms for viscous losses in a turbomachinery tip-clearance flow, J. fluid mech. 586(2007) 177-204.

[14] W.M. Batten, N.W. Bressloff, S.R. Turnock, From vortex to wall driven turbulence production in the Taylor-Couette system with a rotating inner cylinder, Int. J. Num. Met. Fluids 38(2005) 212-223.

[15] Y.S. Ke, C. Ma, Prediction method for blade tip clearance flow of rim driven propulsor, Applied science and technology 46(2019) 6-10. (in Chinese)

[16] E. Bilgen, R. Boulos, Functional dependence of torque coefficient of coaxial cylinders on gap width and reynolds numbers, J FLUID ENG-T ASME 95(1973) 122-126.

[17] D.P. Lathrop, J. Fineberg, H.L. Swinney, Transition to shear-driven turbulence in couette-taylor flow. Phys. Rev. A, 46(1992) 6390-6405.

[18] J.W. Daily, R.E. Nece, Chamber dimension effects on induced flow and frictional resistance of enclosed rotating disks, J. basic eng. 82(1960) 217-230.
[19] Q.M. Cao, X.Z. Wei, D.H. Tang, F.W. Hong, Study of gap flow effects on hydrodynamic performance of rim driver thrusters with/without pressure difference. Chinese Journal of Hydrodynamics 30(2015) 485-494. (in Chinese)
[20] Q. Zhao, CFD simulation of performance for duct propeller and ship wake. Wuhan university of technology, (2011). (in Chinese)
[21] Y. Chen, L. Wang, H.X. Hua, Longitudinal vibration and unsteady thrust transmission of the rim driven thruster induced by ingested turbulence, Ocean Eng. 131(2017) 149-161.
[22] B.W. Song, Y.J. Wang, W.L. Tian, Open water performance comparison between hub-type and hub-less rim driven thrusters based on CFD method, Ocean Eng. 103(2015) 55-63.
[23] A.J. Dubas, N.W. Bressloff, S.M. Sharkh, Numerical modelling of rotor-stator interaction in rim driven thrusters, Ocean Eng. 106(2015) 281-288.